SOLID PARTICLE TRANSPORT BEHAVIOR AND THE EFFECT OF AEROSOL MASS LOADING ON PERFORMANCE OF A SLIT VIRTUAL IMPACTOR

A Thesis

by

SATYANARAYANAN SESHADRI

Submitted to the Office of Graduate Studies of
Texas A&M University
in partial fulfillment of the requirements for the degree of

MASTER OF SCIENCE

May 2004

Major Subject: Mechanical Engineering

SOLID PARTICLE TRANSPORT BEHAVIOR AND THE EFFECT OF AEROSOL MASS LOADING ON PERFORMANCE OF A SLIT VIRTUAL IMPACTOR

A Thesis

by

SATYANARAYANAN SESHADRI

Submitted to Texas A&M University
in partial fulfillment of the requirements
for the degree of

MASTER OF SCIENCE

Approved as to style and content by:

Denis J. Phares (Chair of Committee)	Kenneth D. Kihm (Member)
Peter M. McIntyre (Member)	Dennis L. O' Neal (Head of Department)

May 2004

Major Subject: Mechanical Engineering

ABSTRACT

Solid Particle Transport Behavior and the Effect of Aerosol Mass Loading on Performance of a Slit Virtual Impactor. (May 2004)

Satyanarayanan Seshadri, B.E., University of Madras, Madras, India

Chair of Advisory Committee: Dr. Denis J. Phares

Transport of solid particles in a slit virtual impactor has been analyzed using visualization techniques. Particle trajectories were observed using laser-induced fluorescence of monodisperse particles seeded in the virtual impactor flow. It was observed from these trajectories that for smaller inertia particles essentially followed the flow streamlines, whereas higher inertia particles tend to deflect from their initial streamlines. These transport characteristics were used to determine particle collection efficiency curves, and the percentage of *defect* particle transmission, particles transmitted to the major flow that are well beyond the experimentally determined 50% cutoff. Defect percentages were found to be in good agreement with those based on a local stokes number approach, an analytical model using a converging flow velocity profile. It was hypothesized that these defects occur by virtue of larger particles passing through the near wall flow region and consequently transported to the major flow. The trajectories of such defect occurrences clearly show that these particles originated in the near wall region.

Performance at higher mass loadings was evaluated using a background dust matrix generated by a turntable aerosol generator. At high mass loadings, clogging of the slit led to the deterioration of the impactor's performance. The time taken to clog the silt was

estimated by modeling the slit edge as a single filter fiber of rectangular cross section with the primary mechanism of filtration being interception and was found to be in good agreement with the experimental data. Elimination of defect transmission and clogging would be possible by the provision of a sheath airflow, which ensures that the near wall regions are free of particles.

DEDICATION

To my parents, for their unfailing love and trust in me

ACKNOWLEDGEMENTS

At this juncture, when my pursuit towards a master's degree is nearing fruition, I would like to express my heartfelt thanks to everyone who backed me in this endeavor. I would like to express my sincere appreciation to Dr. Denis Phares for his constant support, both financial and intellectual, throughout the program. I thank him for his trust in my capacity and for entrusting me with this important project. I would like to thank Dr. Peter McIntyre for being on my committee and for his support during my brief stint at Accelerator Technology Corporation. I would also like to thank him for his meaningful discussions and insights that helped me succeed in this research. I would like to thank Dr. Kenneth Kihm for being on my committee and for the various resources he provided for the success of this research. I would like to express my thanks and well wishes to Mr. Taekyun Kim, with whom I shared the jubilation and tribulations of this research. I would like to express my sincere gratitude to my father Mr. S. Seshadri and to my mother Smt. Sudha Seshadri, for their immense support and sacrifices that have helped me realize my goal. I will always cherish the light and relaxing moments that I had at Texas A&M in the company of very good friends like Shankar, Gaurav and Stan. Finally, I would like to thank the Department of Mechanical Engineering, of which I will be a proud alumnus, for providing me this opportunity for higher education in Aggieland.

TABLE OF CONTENTS

	Page
ABSTRACT…….……..	iii
DEDICATION……...	v
ACKNOWLEDGEMENTS……...	vi
TABLE OF CONTENTS……...	vii
LIST OF FIGURES……...	viii
LIST OF TABLES…….	x
1. INTRODUCTION……...	1
Particle Classification in a Virtual Impactor……...	3
2. EXPERIMENTAL…….…..	7
Vibrating Orifice Aerosol Generator……..	8
Virtual Impactor…….….	10
Turntable Dust Generator……...	13
3. RESULTS……	16
Collection Efficiency……..	16
Effect of Initial Approach Angle on Collection Efficiency……	18
Visualization of Particle Trajectories……..…	18
Effect of Mass Loading……...	22
4. DISCUSSION……..	25
Characteristics of Convective Transport…….	30
Mechanism of Clogging in Slit Virtual Impactor – Rectangular Filter Fiber Analogy…….....	32
5. CONCLUSION……	38
REFERENCES……..	40
VITA……..…	42

LIST OF FIGURES

FIGURE		Page
2.1	Component design based on geometric optics (Schematic of laser illumination)……..	7
2.2	Cross section of Vibrating Orifice Aerosol Generator……...…	8
2.3	Test for monodispersion. a) a straight jet, b) monodisperse configuration c) polydisperse configuration …….	8
2.4	Images of generated particles, collected over a microscopic cover glass …….	10
2.5	Prototype unit a) photograph, b) schematic and area under investigation……...	11
2.6	Schematic and picture of Turntable Dust Generator……..……	14
2.7	Dust output as a function of time for one revolution of turntable..	15
3.1	Collection efficiency at the major flow as a function of $Stk^{0.5}$…..	17
3.2	Particle trajectories at lower Stokes number (D_p = 4.8 μm, Stk = 0.2, Airflow rate = 0.29 SCFH, Re = 6.3)……	20
3.3	Particle trajectories at higher Stokes number (D_p = 9 μm, Stk = 50, Airflow rate = 20.33 SCFH, Re = 448) ……...	21
3.4	Visualization of mixture of Arizona Road Dust (ARD) and Fluorescent Particles (FP)……..…	23
3.5	Condition of slit at various mass loadings, after two minutes of operation…….	24
4.1	Defect particle transmissions at airflow rate = 20.33 SCFH, Re = 448……..	26
4.2	Velocity profile for a converging channel flow at the designed flow rate ($\dot{Q}_{air}$ = 7.51 × 10^{-5} m^3/s)……	27

FIGURE Page

4.3 Local Stokes numbers for smaller particles, based on a converging channel velocity profile for $\dot{Q}_{air}$ = 7.51 × 10^{-5} m^3/s... 28

4.4 Local Stokes numbers for larger particles, based on a converging channel velocity profile for $\dot{Q}_{air}$ = 7.51 × 10^{-5} m^3/s.……. 29

4.5 Schematic of particle behavior based on their size (Stokes number)…….. 31

4.6 Single fiber representation of slit edge and the control volume under investigation……. 32

4.7 Number distribution plots for ARD and Bi-2223 precursor powder…… 35

LIST OF TABLES

TABLE		Page
2.1	Standard deviation in size of particles generated using the VOAG……	10
2.2	Dust generator output as a function of turntable speed and inlet pressure……..	13
3.1	Experimental collection efficiency for the virtual impactor……..	17
3.2	Experimental dust loading conditions..…….	22
4.1	Comparison between measured and predicted collection efficiency……	30
4.2	Clogging time, comparison between experimental and analytical results ……	37

INTRODUCTION

The size of particulate matter dictates their transport and chemical properties and is thus a critical parameter in a number of environmental and industrial processes. With the lower limit of collection and measurement devices being pushed to the nano-scale, it becomes imperative to have devices that are capable of separating particles beyond a certain threshold with near 100% efficiency. This is particularly true in semiconductor fabrication, wherein the dimensions of the components are comparable to that of a small dust particle, whose presence may lead to failure of the component. Environmentalist and health scientists are particularly interested in very small particles, as ultrafine aerosol have been shown to be responsible for a wide range of adverse health effects. In 1995, Pope et al., (1995) reviewed the health effects of particulate air pollution and concluded that it is an important contributing factor for respiratory diseases. He observed that the general health effects include a decreased lung function and increased cardiopulmonary disease mortality. Oberdorster and Utell (2002), in their editorial for environmental health perspectives, outlined the changing perspectives of scientists throughout the world towards ultrafine particulate matter (size < 0.1μm). They discussed the potential health hazards due to automobile particulate exhausts and presented some outcomes from preliminary clinical trails. Mechanisms by which these particles can be concentrated and collected are needed for analyzing the effect of these particles. The virtual impactor is

---

This thesis follows the style and format of *Aerosol Science and Technology*.

one such device, which separates particles from the air stream based on its aerodynamic size. Most of the research so far has focussed on collection of particles above a particular size. Numerous works have been done on the development of high efficiency virtual impactors (Loo and Cork 1988, Sioutas et al. 1994) and methods to enhance its collection efficiency (Chen and Yeh 1987, Gotoh and Masuda 2000) of the larger particles.

There are a few applications, which focuses on particles with sizes below the threshold. Powder-in-tube (PIT) fabrication of multi-filament superconducting wires and tapes is one such application. In a recent study, Fu et al. (2003) suggested using a virtual impactor to filter out particles larger than a prescribed threshold from a batch powder, thereby replacing sieving. The distribution of particle size in the precursor powder plays a particularly important role in limiting the ultimate current density that can be attained. The super-currents are carried predominantly in the interfaces between the core and the matrix. Thus fabricating filaments with larger number of finer filaments could increase the current density. The limiting factor in drawing out the finest possible mono-filament, which is prepared by packing powder of superconducting material (core) in to a metal tube (matrix) typically silver or copper and drawn down to the required size, is the largest particle size in the core powder. Typically the core powder is much harder than the matrix metal, so during drawing as the tube size approach the diameter of the largest particle in the filling, that particle is more likely to pierce the wall of the tube. When the conductor is then heat-treated, the filament and the surrounding matrix are ruined. The synthesized precursor powder has a stochastic distribution in particle size with mean typically in the range of a few microns but with tails to the distribution that extend to 10

micron or more. Even a few such large particles could ruin the performance of the superconductor. Thus it would be desirable to remove all large particles prior to filling up the powder in to the tubes. In order to extend virtual impact processing technique to process precursor powder, it is essential to understand individual particle behavior and its separation characteristics in a virtual impactor. Although fundamental operation of a virtual impactor has been discussed in a number of papers, behavior of single particles and its effect on the separation efficiency have not been studied.

Particle Classification in a Virtual Impactor

Virtual impactor is a device used for inertial separation of airborne particles. It can classify particles according to the aerodynamic size. In this type of impactor, a region of relatively stagnant fluid replaces the impaction plate. This is accomplished by splitting the gas flow just downstream of the jet nozzle in to a major flow, drawn perpendicular to the jet nozzle, and a minor flow drawn parallel to the direction of the original flow. Only a small fraction (typically 10% of the total flow) of the fluid flow is drawn into the minor flow to ensure a strong fluid deflection within the region of particle separation. Particles larger than a certain size (or the cut-off size) has sufficient inertia to cross the fluid streamlines are introduced in the minor flow and those that are less than the cut off size follow the deflected streamlines. The principle parameter determining inertial separation of a particle with diameter, d_p, is the Stokes number, *Stk*, where the characteristic length is generally taken to be half of the slit width, *W*:

$$Stk = \frac{\tau U}{D_j} = \frac{\rho_p C_c d_p^2 U}{9 \mu W}, \qquad (1.1)$$

where U is the average jet velocity, ρ_p is the particle density, μ is the dynamic viscosity, and the Cunningham slip correction, C_c, is equal to 1 under normal operating conditions. Stokes number can be defined as the ratio of stopping distance of particle to the characteristic dimension of the flow restriction. In other words, it can be described as the ratio of characteristic particle response time to the flow response time. Physical significance of Stokes number is that it represents the ability of the particle to adjust to the changing flow fields. Ideally, particles having a Stokes number lesser than or equal to one adapt to the abruptly changing streamlines easily and follow them. At larger Stokes numbers, particle slip occurs due to particle containing larger inertia.

Virtual impactors were primarily developed to eliminate the particle bounce and re-entrainment problems associated with conventional inertial impactors. Marple and Chein (1980) evaluated the performance and collection efficiency for round and rectangular nozzle virtual impactor by numerical solution of Navier-Stokes Equation and the equation of motion for particles. They analyzed the effect of nozzle Reynolds number, fraction of flow passing through collection probe, probe width, nozzle throat length, nozzle to probe distance and probe inlet design on the collection efficiencies of small and large particles. Only nozzle Reynolds number had a significant effect on larger particle collection, however, smaller particle collection efficiency was affected by many of these parameters. Chen and Yeh (1987) and Loo and Adachi (1979) investigated the performance of a dichotomous slit virtual impactor and obtained the separation efficiency as a function of Stokes number. Their reported 50 % cutoff Stokes numbers are 0.4761

and 0.6889 respectively. Sioutas et al., (1994) designed a slit virtual impactor having a low cut point, to separate particles in the range 0.1 – 0.25 microns.

Separation characteristics of a virtual impactor can be better understood by visualizing the convective transport of the separating particles. Flow fields for various Reynolds numbers in a water model virtual impactor has been obtained by Marple and Chein (1980) using electrolytic flow visualization technique to validate their numerically generated flow field. Han and Mosses (1997) visualized the flow fields in the virtual impactors using dye streams to study the effect of central clean water flow rate and the minor flow rate on the stability of flow stream lines in the dichotomous region. Gotoh and Masuda (2000) attempted to visualize solid particles in a rectangular jet virtual impactor to study the effect of flow characteristics on the performance of virtual impactors. Although this research gives an insight into solid particle behavior in virtual impactors, it dose not represent the true behavior as experienced in practical situations wherein virtual impactors are most often used for separating particles from gas streams. Thus it becomes necessary to visualize particle transport in a gas flow as no such attempt has been made before.

The viability of a slit virtual impactor as a large particle filter for PIT applications requires, 1) the elimination of the transmission to the major flow of any particle larger than a prescribed cutoff diameter (defect), and 2) the ability to operate at high particle mass loadings without performance degradation. To address the first concern, individual defect events are characterized in order to apply measures to minimize the onset of such events.

It can be hypothesized that defects may occur due to large particles that may travel through the fluid boundary layer close to one of the walls in the device. This would cause that particle to enter the separation region with a smaller velocity than those particles in the free stream of the fluid, and consequently may more easily negotiate the turn into the major flow. To address the second concern, VI's performances at higher aerosol mass loadings were evaluated to determine loading conditions, which would degrade its performance. Particle – wall interaction and particle – particle interaction effects are pronounced thereby leading to deterioration in performance due to clogging of the slit. Clogging, primarily due to interception, could occur when particles travel in streamlines that are within one particle radius from the nozzle surface. Using the concept of filtration by a single fiber, the slit edge was modeled as a single fiber with rectangular cross-section. The total particulate collection efficiency of the rectangular or cylindrical fiber, taking in to account the initial particle size distribution, was discussed in detail by Zhu et al. (2000). It can be reasoned that clogging would occur if the total projected surface area occupied by the particles collected on the slit edge is equal to the cross sectional area of the slit opening. Using a log-normal initial particle size distribution, the total time it would take for the clogging of the impactor was evaluated for the designed flow rate and compared with the experimental data.

EXPERIMENTAL

The experimental setup consists of an optical illumination system, a particle generation system, the virtual impactor, and an image recording and processing system. For the mass loading experiments, a turntable dust generator was built based on a design by Reist and Taylor (2000). As shown in figure 2.1, a laser beam is split into two laser sheets, as described by Hecht (1998) to simultaneously illuminate two sides of the virtual impactor. Two different lasers were used during the study: a solid state pulsed Nd:YAG laser GCR-12 (Spectra-Physics) (532 nm, 155 mJ/cm^2) and a continuous-wave (CW) Argon-Ion laser. The CW laser generates wavelengths between 488 nm and 515 nm with an output of 210 mW at whole spectrum and 32 mW at 488 nm.

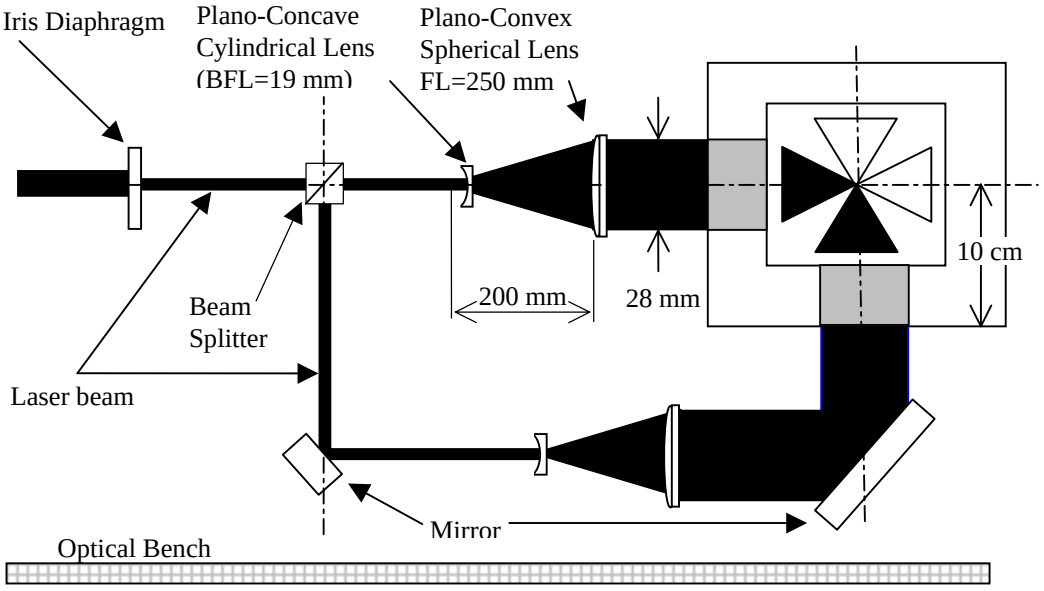

FIGURE 2.1. Component design based on geometric optics (Schematic of laser illumination)

Vibrating Orifice Aerosol Generator

Monodisperse fluorescent particles were generated using a modified vibrating orifice aerosol generator (VOAG); similar to that described by Levindis and Flagan (1987), that is compatible with organic solvents. A schematic of the system is shown in figure 2.2. Breaking up of the jet in to monodisperse droplets was achieved using acoustically induced disturbances from a piezoelectric biomorph crystal epoxied to the back of a stainless steel shim stock.

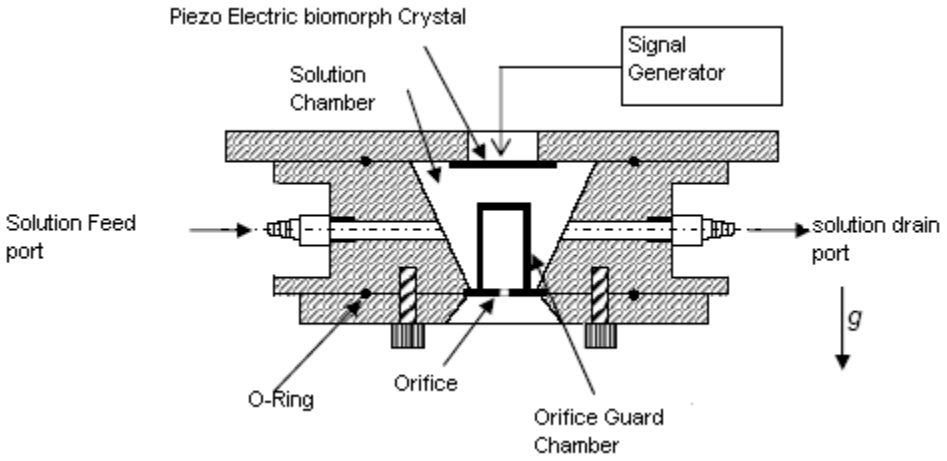

FIGURE 2.2. Cross-section of Vibrating Orifice Aerosol Generator (VOAG)

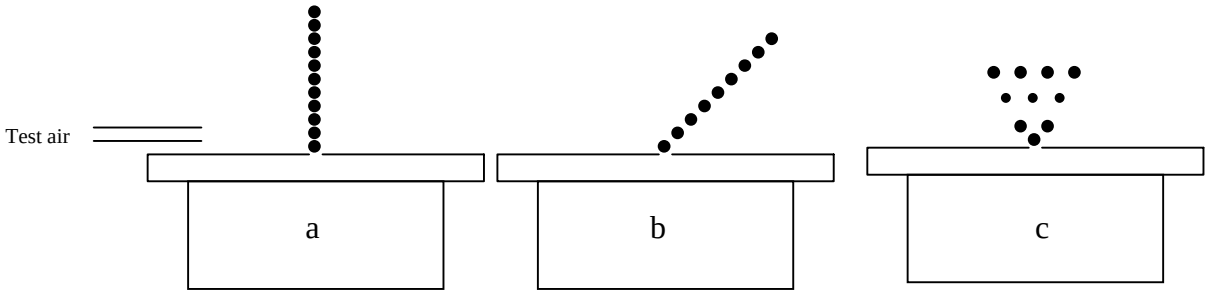

FIGURE 2.3. Test for monodispersion. a) a straight jet, b) monodisperse configuration c) polydisperse configuration

Monodisperse droplets are produced at certain resonant frequencies that break up the jet in to uniform size droplets. This was verified using a test air as shown in Figure 2.3. When the breakup is uniform, the liquid droplet stream bends like a single wire as shown in the figure 2.3b. In other cases, the dispersion under test air is just like a spray as shown in figure 2.3c. Particles of various sizes were obtained by varying the solution concentration. A 10 and 20-micron orifice were used to generate the solution droplets, depending on the desired particle size. The frequency of the sinusoidal wave for uniform breakup varied between 21 and 30 kHz for 20 and 10 μm orifices respectively. Generated droplets were dispersed and dried by mixing it with dispersion and dilution air in the drying column. Dispersion and dilution airflow rates were varied to optimize the shape of the generated droplet. Solid fluorescent particles in the range 1.22 to 9 microns were generated from alcohol soluble fluorescein dissolved in isopropanol. For the mass loading experiments, Rodhamine 590 dissolved in ethanol was used to generate the solid particles as it could be exited by the Nd:YAG laser. The sizes of the particles that were generated during each experiment were verified using an Olympus BX61 (reflected fluorescence) microscope, equipped with a CCD camera and NIH imaging software. Figure 2.4 shows fluorescent particles collected on a microscopic cover glass, under the microscope. Table 2.1 shows the standard deviation for different particle sizes. The standard deviation of the generated particles varied between 0.4 to 0.9 microns with the mean at 0.49 microns. The VOAG was mounted directly on top of the virtual impactor to minimize gravitational losses in transport channels.

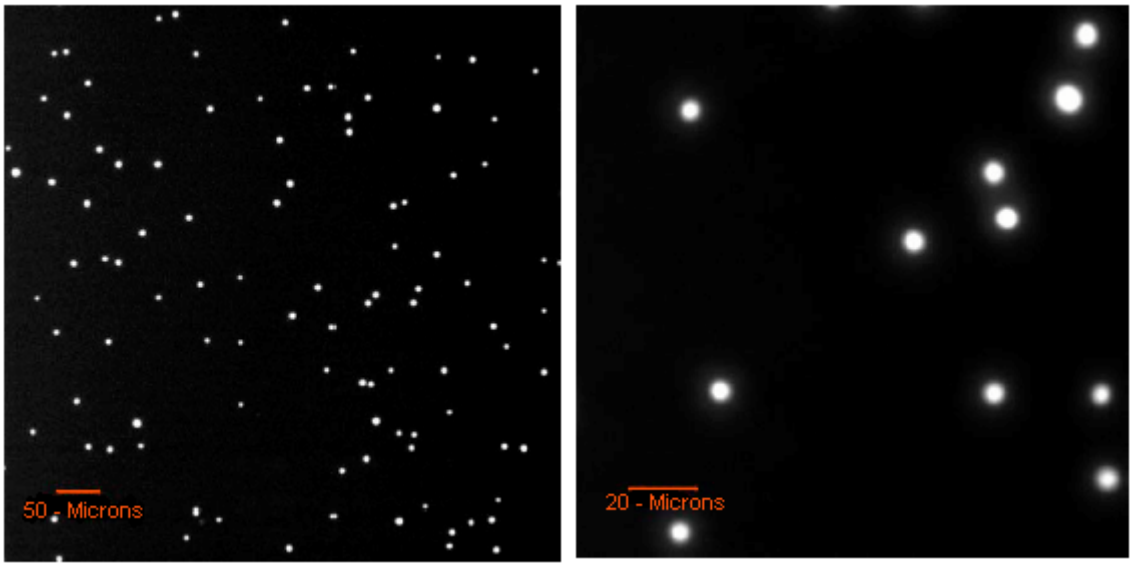

a) Using 10X magnification b) Using 40X magnification

FIGURE 2.4. Images of generated particles, collected over a microscopic cover glass

TABLE 2.1. Standard deviation in size of particles generated using the VOAG

$D_{p,ave}$	1.2	4.0	4.4	4.8	5.4	7.3	9	σ_{ave}
σ (μm)	0.33	0.39	0.40	0.42	0.32	0.98	0.6	0.491

Virtual Impactor

The virtual impactor that was used for this visualization study was designed based on a high-volume slit virtual impactor presented by Ding et al. (2001). The present device was machined to very high tolerance out of Stainless Steel using wire EDM. Figure 2.5 shows a schematic and picture of the prototype used for this study. The virtual impactor used in this study was designed to have a converging flow with a 60-degree angle. The prototype unit was enclosed in an airtight Plexiglas housing with one inflow and three

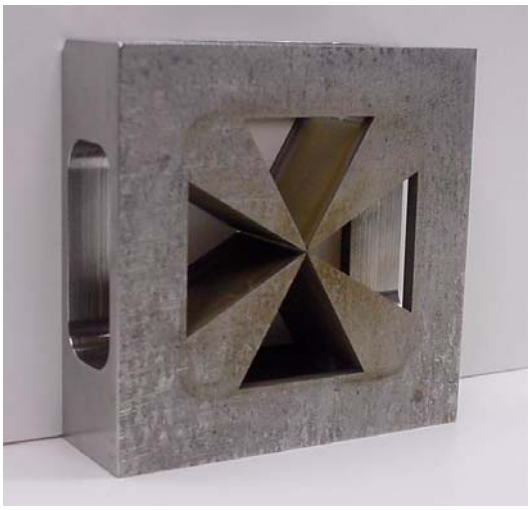

a) Photograph of VI used for visualization

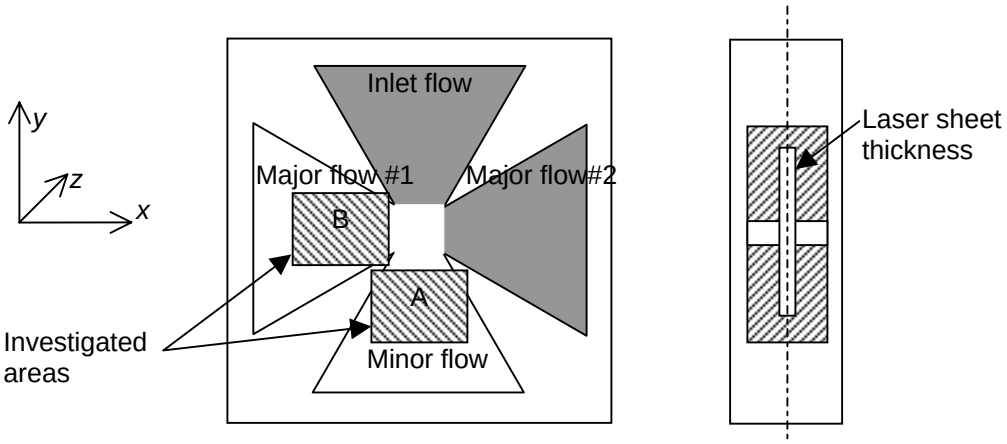

b) Schematic of VI used for investigation

FIGURE 2.5. Prototype unit a) photograph, b) schematic and area under investigation

outflow ports. Glass windows were provided on all sides for laser illumination and observation. Airflow through the virtual impactor was driven through suction from a downstream blower and the individual flow rates were controlled using flow rotometers.

A CCD camera oriented perpendicular to the laser sheet was used to detect either the scattered light or fluorescence of the particle; the images were recorded onto a VHS tape and to a PC using a frame grabber. Analog images from the VHS tape were later digitized for further analysis using a Sony digital video converter and the images were analyzed using Adobe Premiere^{tm} 6, a movie editing software. Although using a PC with frame grabber can directly provide digital images, VHS tapes were used to provide high resolution images and also to store large amounts of data. Solid particle trajectories through the virtual impactor were visualized for 4, 4.8 and 9-micron particles. The Stokes number was maintained by regulating the flow through the impactor. These experiments were followed up with the mass loading experiments, wherein varying amounts of ARD mixed with Rodhamine 590 was fed in to the impactor. The major and minor flows were visualized as before using Nd:YAG laser.

Turntable Dust Generator

A dry dispersion aerosol generator was built in the lab for conducting the mass loading experiments. It was based on the improved turntable dust generator design by Reist and Taylor (2000). Figure 2.6 shows a schematic of the dust generator. A rotating dust cylinder ensured steady delivery of dust to the turntable groove, from where it was picked up by a venturi aspirator. The dust loading could be varied either by adjusting the air pressure or the turntable speed. The dust feeder was calibrated for total mass of the dust output based on different turntable speeds two different operating pressures. Figure 2.7 shows the calibration plots for different inlet pressures. The output could be increased either by increasing the inlet air pressure or by increasing the turntable speed. The output from the feeder was connected to an inline 47mm filter and the loadings were determined from the initial and final mass of the filter paper. Table 2.2 shows the calibration data for two operation pressures and different turntable rotation rates.

TABLE 2.2. Dust generator output as a function of turntable speed and inlet pressure

Input Pressure (psig)			
18		20	
Time taken for one revolution (s)	Mass output (μg/l)	Time taken for one revolution (s)	Mass output (μg/l)
8	1249.27	14	1523.50
25	977.31	30	1339.67
39	742.64	92	571.68
60	430.32		

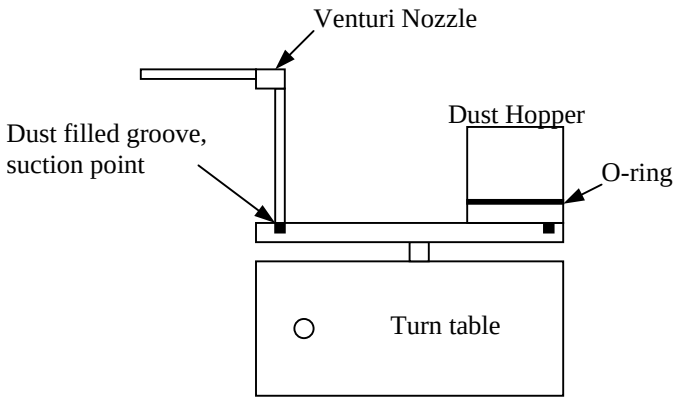

a) Schematic of Turntable Dust Generator

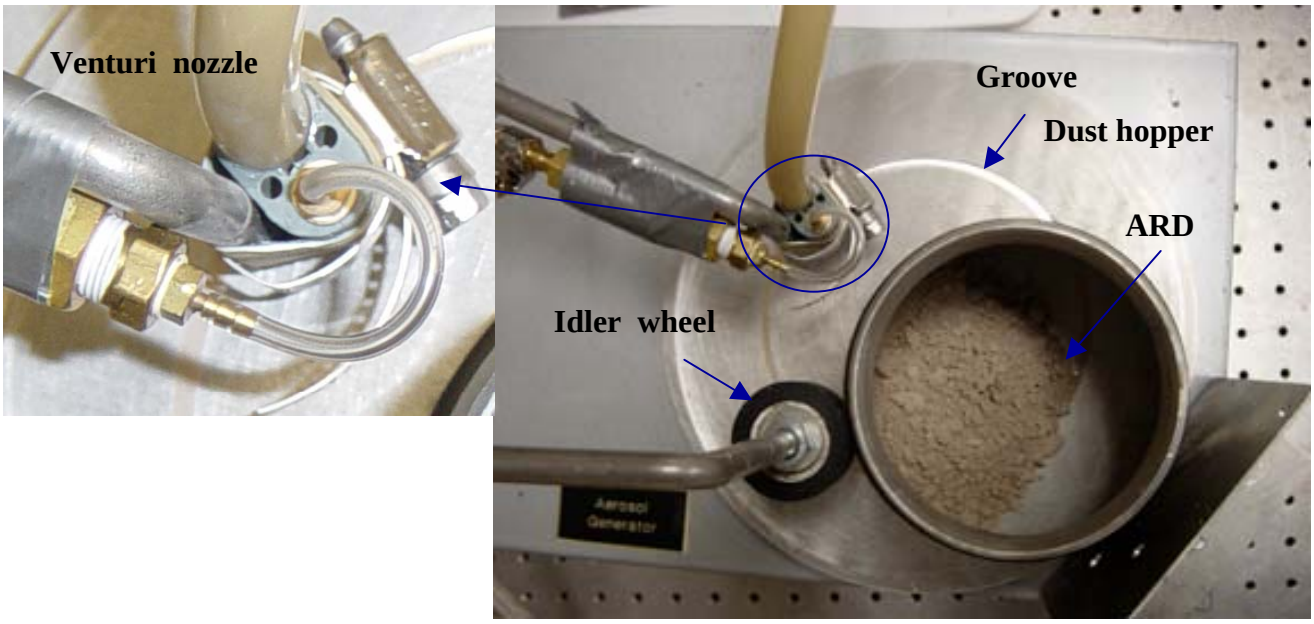

b) Picture of Turntable Dust Generator

FIGURE 2.6 Schematic and picture of Turntable Dust Generator

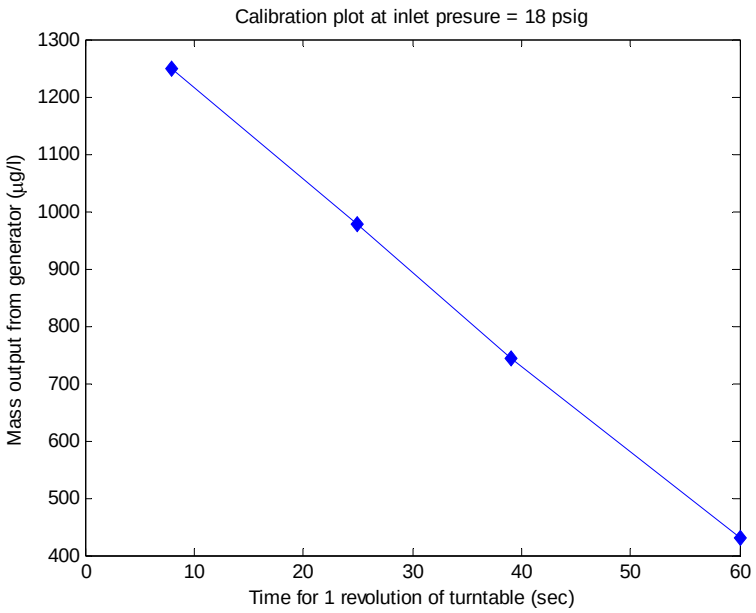

a) Inlet pressure = 18 psig

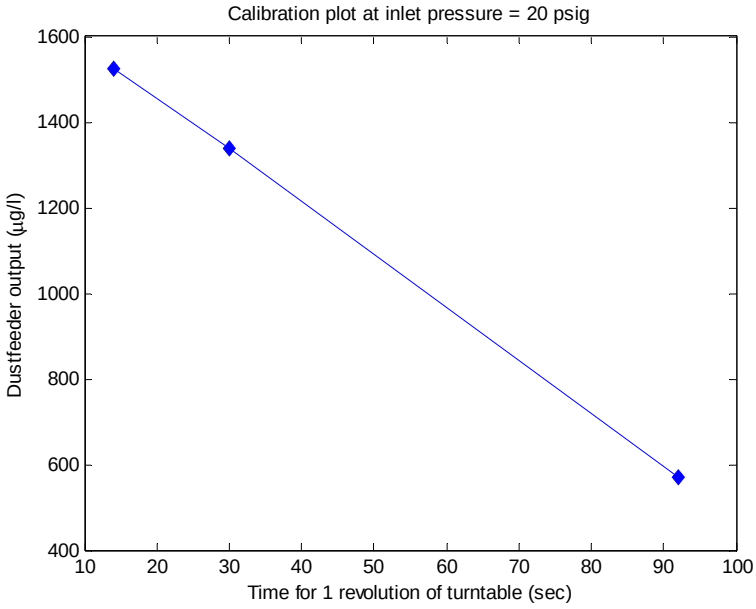

b) Inlet pressure = 20 psig

FIGURE 2.7. Dust output as a function of time for one revolution of turntable

RESULTS

Collection Efficiency

The critical size or the cut off particle size is defined as that for which the particles equally divide between the major and the minor flow and is characterized by Stokes number as shown in equation (1.1). Under identical conditions Stokes number is a function of particle size only. The ratio of major to minor flow rates were maintained at 9:1 for all experimental investigations, while actual flow rates were varied to adjust the particle Stokes number. The collection efficiency at the major flow calculated based on the experiments is given by

$$\eta_{\text{major flows}} = \frac{(\#\ \text{of particles in major flow 1 per frame}) \times 2}{(\#\text{of particles in major flow 1 per frame}) \times 2 + \#\ \text{of particles in minor flow per frame}} \quad (3.1)$$

Experimental measurement of particle number density or the corresponding number of particles per frame, in the major and minor flows is presented in table 3.1. The efficiency curve is plotted based on these data and is shown in figure 3.1. It also shows a comparison between our results and those of Loo and Cork (1979) and Chen and Yeh (1987). It demonstrates a sharper cutoff with the 50% cut point at a Stokes number of 0.82. Though theoretical models preclude the presence of larger particles in the major flow beyond the 50% cutoff size, we do find a small percentage of larger particles in the major flow. As the presence of these defect particles is detrimental to the performance of the superconducting wire, trajectories of different particle sizes were visualized the through the impactor using CW-Argon ion laser so as to apply any corrective measures later.

TABLE 3.1. Experimental collection efficiency for the virtual impactor

Stokes Number (Stk)	Major flow (Left)		Minor flow		Collection efficiency at minor flow (%)
	Average number of particles per frame	Total number of particles / total number of frames	Average number of particles per frame	Total number of particles / total number of frames	
0.42	0.539	302 / 560	0.175	98 / 560	13.96
0.72	0.96	1028 / 1071	1.08	896 / 830	35.99
0.81	0.70	406 / 582	1.07	646 / 603	43.43
0.92	0.41	331 / 815	3.03	1150 / 380	78.84
1.00	0.082	134 / 1642	2.36	1392 / 591	93.52
7.2	0.107	127 / 1187	10.105	1253 / 124	97.93
9.08	0.07	81 / 1202	15.01	2086 / 139	99.11
16.0	0.007	8 / 1200	22.00	594 / 27	99.94
25.0	0.003	4 / 1213	13.67	902 / 66	99.95

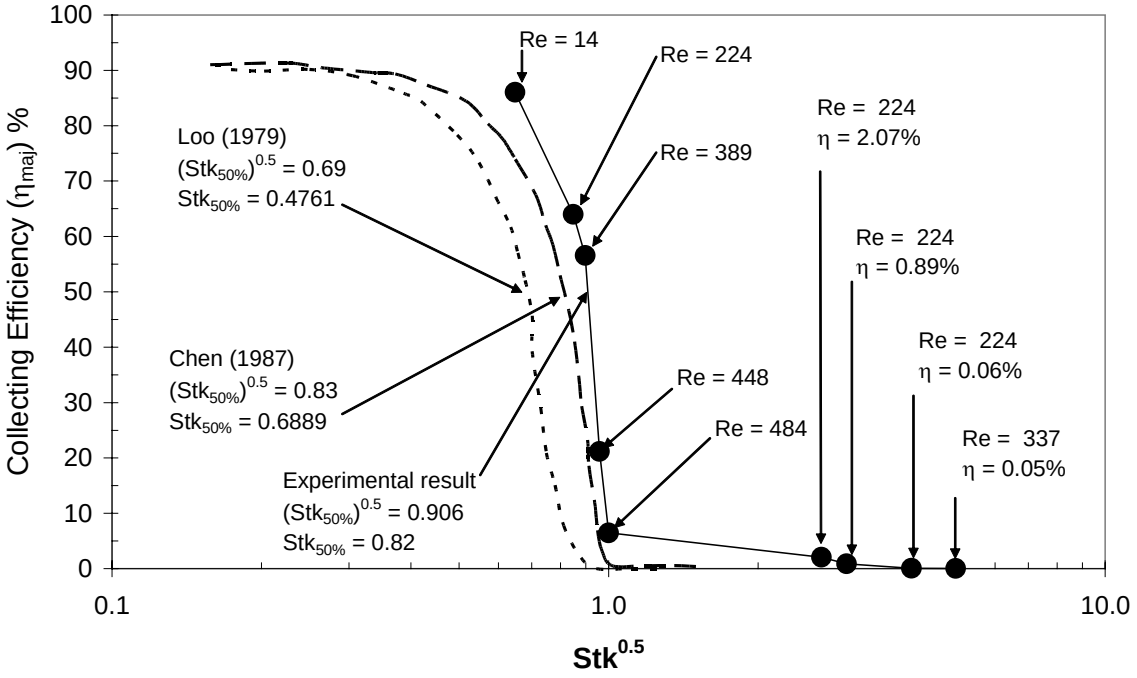

FIGURE 3.1. Collection efficiency at the major flow as a function of $Stk^{0.5}$

Effect of Initial Approach Angle on Collection Efficiency

Marple and Chein (1980), Chen and Yeh (1987) studied the effect of entrance angle on large particle collection efficiency. Marple showed that for larger inlet angles, particles were thrown closer to the centerline, making the collection in the minor flow easier. He found that particle wall-losses were fewer for 90-degree approach than for a 60-degree approach. However, for larger angles, contamination of smaller particles in minor flow increases. This means a larger angle would reduce the effective throughput of smaller particles in the major flow, which may be detrimental to our application. Chen determined that smaller angles at approach increases the cut off size as shown in figure 3.1. Chen compared his efficiency curve at a 60-degree angle of approach to that of Loo and Adachi (1979) 90-degree angle of approach and found that Loo's cut off was lower due to particle thrown towards the center line.

Visualization of Particle Trajectories

The convective transport behavior of solid particles in the virtual impactor was observed using 4, 4.8 and 9 micron particles respectively. CW argon ion laser was used to obtain the particle trajectories. Smaller particle behavior tends to reflect the flow characteristics in the impactor, as their inertia is too weak to deflect from the flow streamline. Though we used a 4.8-micron particle for this experiment, the Stoke's number was maintained at 0.2 by regulating the flow through the impactor. Figure 3.2 shows enhanced images of particle trajectories at lower Stokes number. An individual trajectory represents the particle path for a period of 33 ms per image at 30 frames-per-

second recording rate. It is to be noted from these images that illumination was provided from the bottom. A sheet of laser light having a thickness equal to that of the slit width is permitted in to the inlet flow, which allows for visualization of particles coming within that narrow strip. Only those particles travelling in the narrow strip for the entire recording period (33 ms) can be visualized and any other particle coming on from surrounding flow regions are not seen. Based on these observations, the inlet flow is divided into regions A and B as shown in figure 3.2a and the effects of particle laden in each of these regions are discussed. Although the trajectories in upstream of the inlet are not seen due to limitation in illumination, these can be nevertheless assumed as their traces are visible near the throat region and is also reasonable due to laminar nature of the flow. Figure 3.2b and 3.2c shows the trajectories of particles originating in A and B flow regions respectively. Enlarged image of the intersection as shown in figure 3.2b, particle trajectories that enter the major and minor flows respectively and their relative position in the inlet flow. The distinction between these flow regions progressively diminishes as the Stokes number is increased. This is evident in figure 3.3, which shows particle trajectories at a Stokes number of 50. At these Stokes numbers inertial forces are dominant over the viscous forces, hence we see particles from different locations in the inlet ending up in the minor flow.

One peculiar phenomenon observed at higher Stokes number is that of cross trajectories as seen in figure 3.3b. This demonstrates that particles do not follow the flow streamlines at higher Stokes number and continue on its straight line motion, due to inertia, which results in such crossing trajectories. Even though most of the larger

particles end up in the minor flow, there are certain defect occurrences that can be explained on the basis of a boundary layer effect.

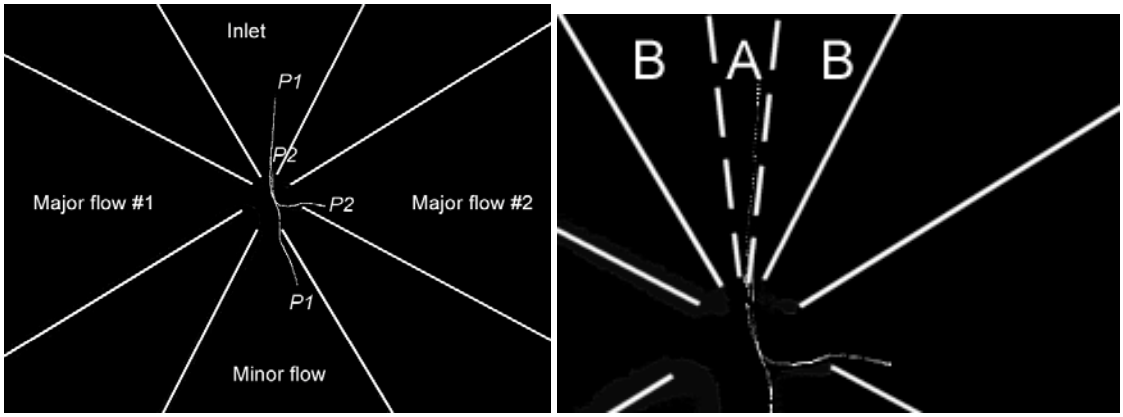

(a)

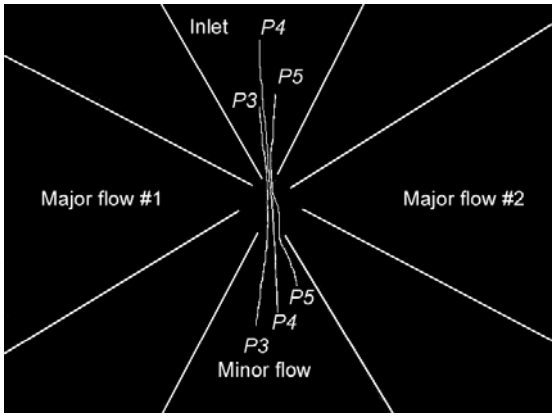

(b)

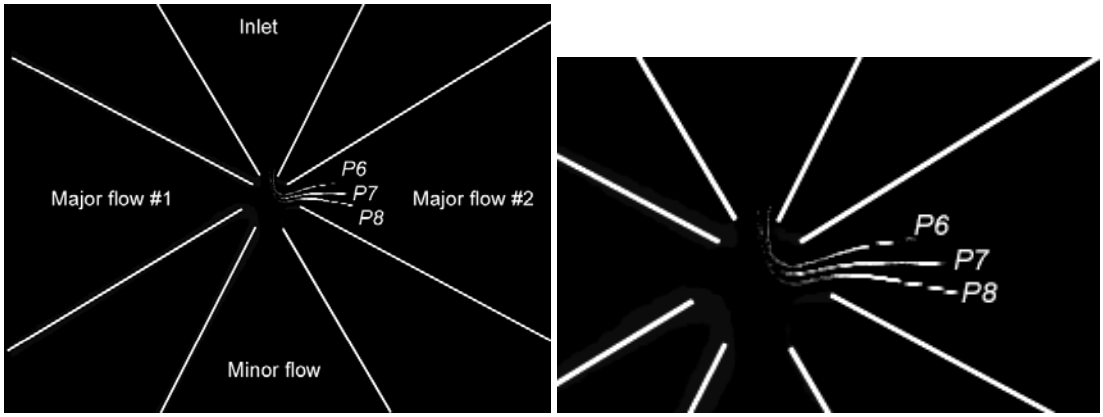

(c)

FIGURE 3.2. Particle trajectories at lower Stokes number (D_p = 4.8 µm, Stk=0.2, Airflow rate = 0.29 SCFH, Re = 6.3)

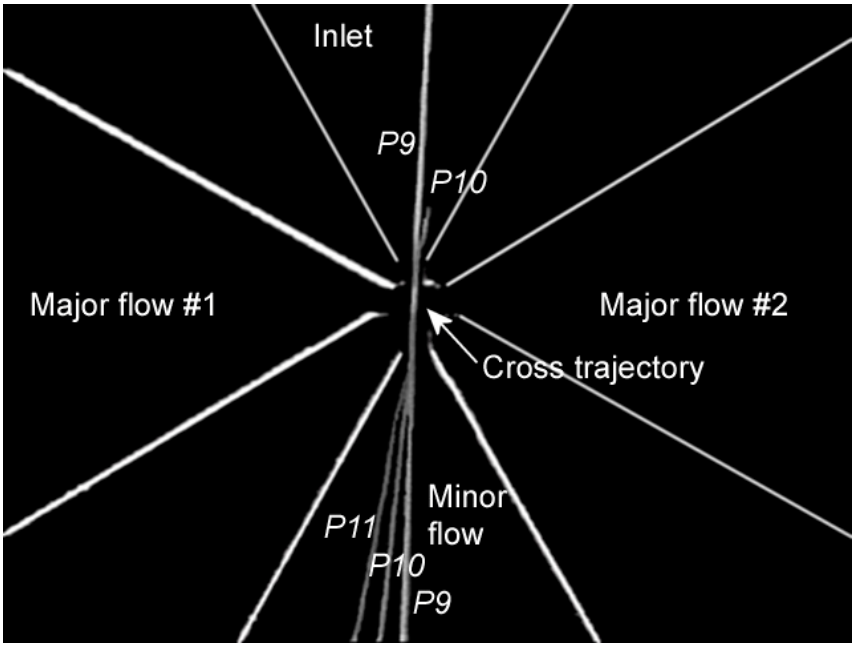

(a)

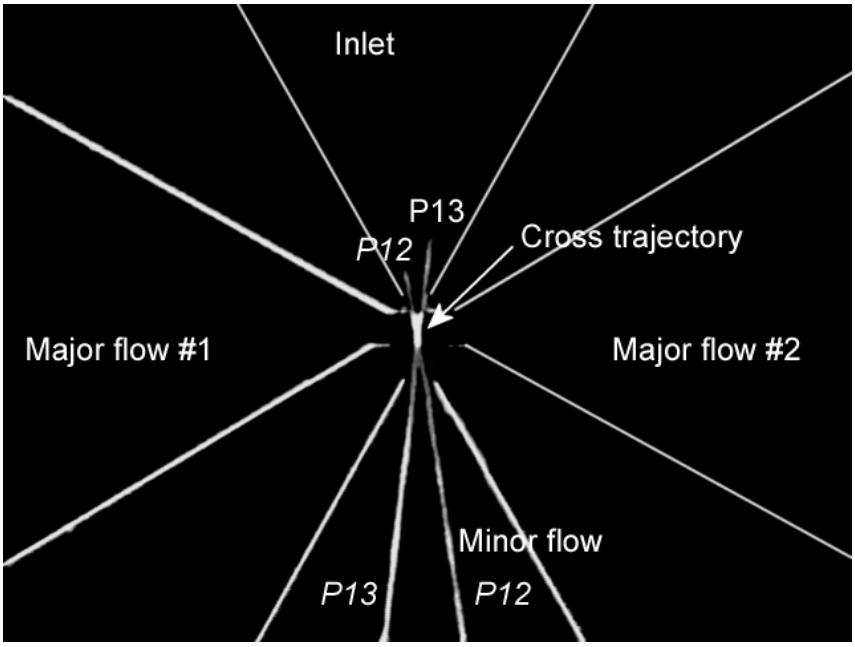

(b)

FIGURE 3.3. Particle trajectories at higher Stokes number (D_p = 9 μm, Stk = 50, Airflow rate = 20.33 SCFH, Re = 448)

Effect of Mass Loading

To study the effect of mass loading, a mixture of ARD and Rodhamine 590 was used and an optical filter was used to filter out the background radiation due to scattering from ARD. Figure 3.4 shows visualization with and without optical filters and was done to verify the effectiveness of the filters. Visualization studies with mass loading enabled us to investigate for additional defects that may be introduced. The performance of the impactor was studied at four different mass loadings. Table 3.2 shows the various loadings at which the impactor was studied. Clogging of the slit in the impactor hindered continuation of this experiment thus bringing about a physical-loading limit beyond which the impactor could not be operated. Figure 3.5 shows slits in the clogged state. It can be seen that there is total clogging of slit for loadings greater than 1200μg/l, and partial clogging occurring for lower loadings. Possible mechanism for clogging and their prevention are discussed later.

TABLE 3.2. Experimental dust loading conditions

Loading	1	2	3	4
μg/l	571.68	977.31	1249.27	1523.50

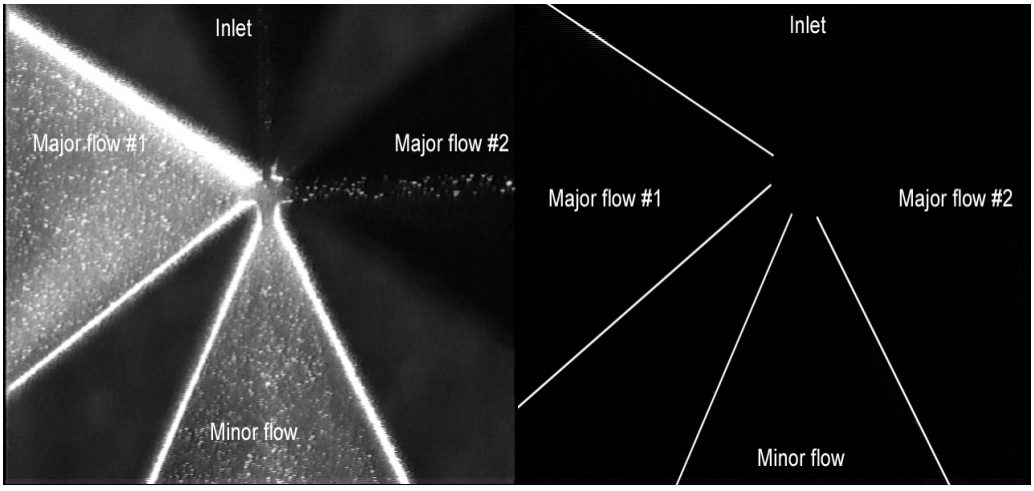

a) ARD without optical filter b) ARD with optical filter

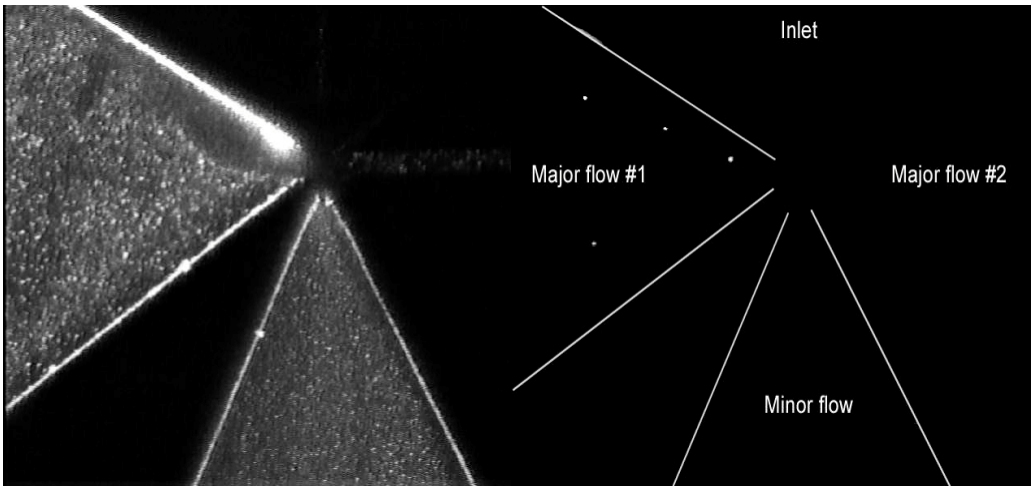

c) ARD + FP without optical filter c) ARD + FP with optical filter

FIGURE 3.4. Visualization of mixture of Arizona Road Dust (ARD) and Fluorescent Particles (FP)

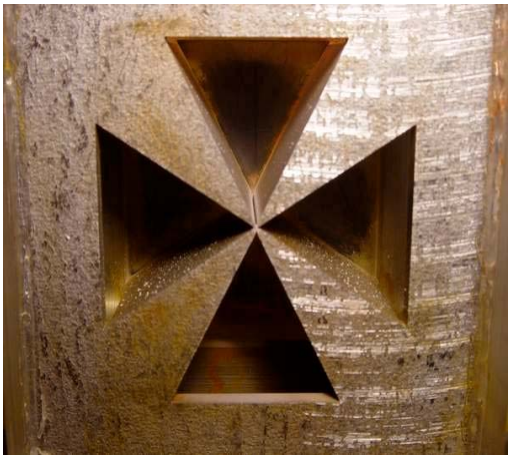

a) 571.68 μg/l Loading

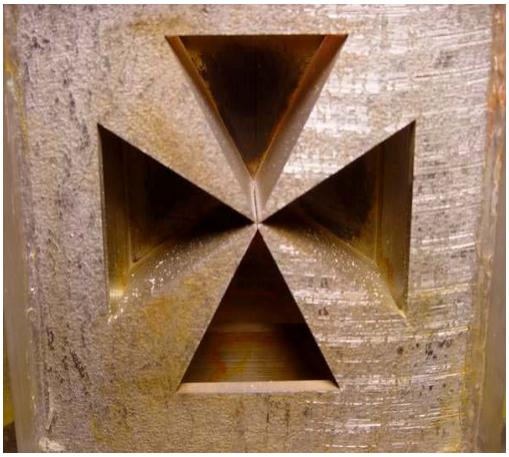

b) 977.31 μg/l Loading

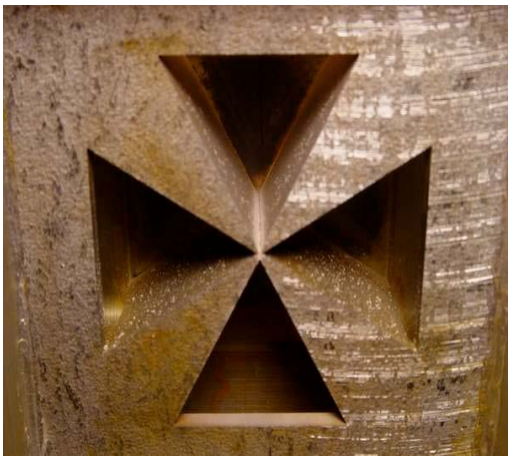

c) 1249.27 μg/l

d) 1523.50 μg/l

FIGURE 3.5 Condition of slit at various mass loadings, after two minutes of operation

DISCUSSION

Often Stokes number is defined based on the bulk velocity through the impactor, based on the airflow rate. For viscous flows however, in regions close to the wall the local flow velocity is much smaller than the mean velocity. This causes particles trapped in these regions to have a very low local Stokes number as compared to the ones out of this layer. This in-turn enables the particles, though larger in size to negotiate the turn to the major flow, thereby resulting in a defect. A straight trajectory from the central region and a defecting trajectory which originated in the near wall region is shown in figure 4.1. Figures 4.1b and 4.1c show defect particle transmission at very high Stokes numbers.

To understand the effects of local Stokes number, we obtained the velocity profile for the converging section using Fluent, a commercial CFD solver. Finite element solution method was applied, quadrilateral shaped elements with a uniform grid spacing of 3.4 X 10^{-5}m, which was 0.1 if normalized with slit width. No-slip boundary conditions were imposed on the side walls and the interior fluid was assigned to be air. Simulations were performed for 600 iterations before the solution converged to within 10^{-3}. Figure 4.2 shows the velocity profile for flow through a 60° converging nozzle at a flow rate of 9.53 SCFH in comparison with the corresponding parallel channel flow having a channel width of $2h_y$, where h_y is the nozzle half width. It is clearly seen that the thickness of the boundary layer in case of a converging nozzle is greatly reduced due to favorable pressure gradients.

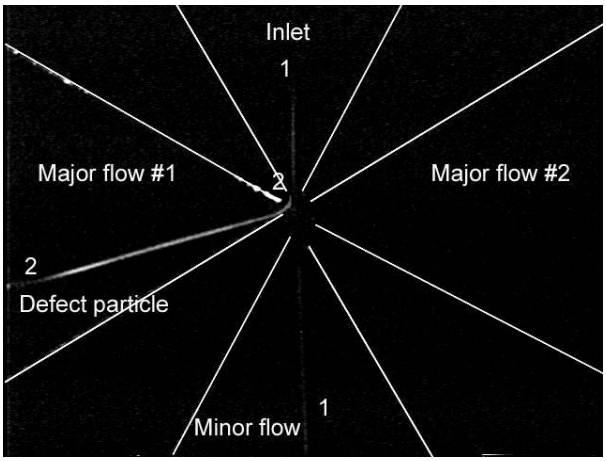

(a) Stk = 10, d_p = 4 μm

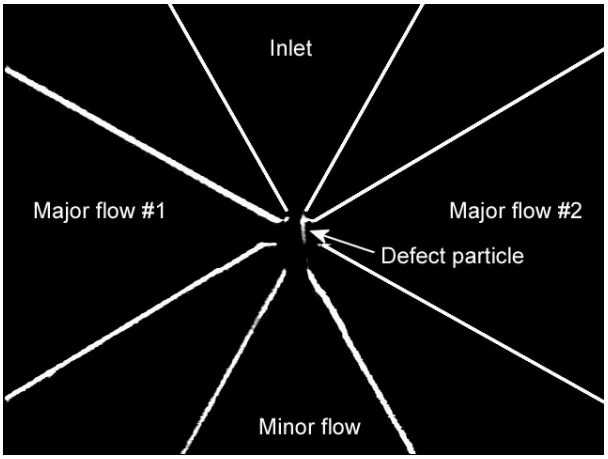

(b) Stk = 50, d_p = 9 μm

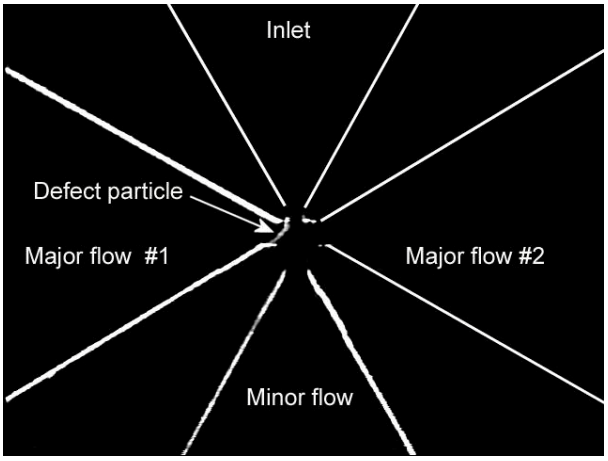

(C) Stk = 50, d_p = 9 μm

FIGURE 4.1. Defect particle transmissions at airflow rate = 20.33 SCFH, Re = 448

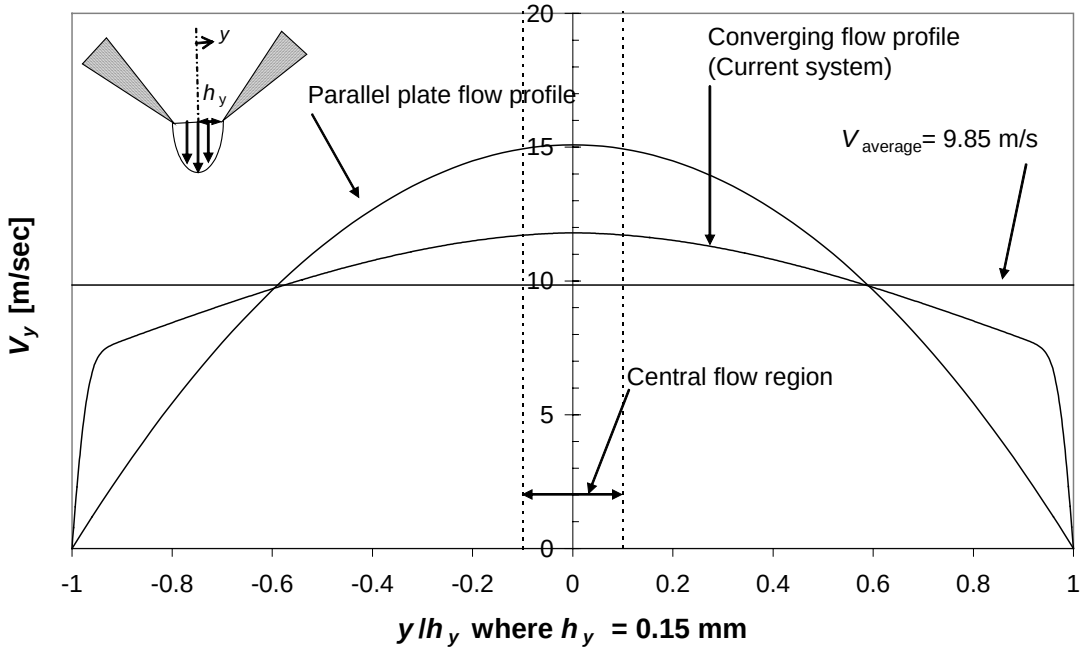

FIGURE 4.2. Velocity profile for a converging channel flow at the designed flow rate ($\dot{Q}_{air}$ = 7.51 × 10^{-5} m^3/s)

For a given particle size, the local Stokes number can be obtained as a function of local flow velocity. Figure 4.3 shows local Stokes number curves for smaller particles, in the range 1.16 to 2.53 μm, based on the converging and parallel channel configurations respectively. The percentage of particles in the major flow that was determined for Stk_{50} = 0.82 using the velocity profile analysis for a converging flow shows reasonable agreement with the experimental data. Thus if the 50% cutoff Stokes number is 0.82, it implies that all particles with Stokes number below this value will follow the flow streamlines and the ones with Stokes number higher than 0.82 will move away from the deflected streamlines due to inertial effects. This implies that for a given particle size, we can analytically determine the percentage of particles which will have a Stokes number less than the 50% cutoff which, should ideally be equal to the percentage of particles in

the major flow. For 1.16 μm particle that has a local Stokes number of 0.42, which is smaller than the Stk_{50} and it is seen that all but the inherent 10% go in to the major flow. Further, for the case of D_p = 2.53 microns, local Stokes number analysis estimates a defect percentage of around 2%, which is comparable to the values obtained experimentally. Table 4.1 presents a summary of experimentally determined collection efficiency for major flow (figure 3.1) and the calculated collection efficiency using local Stokes number approach. Some variation in the theoretically determined collection efficiency may be attributed to our assumption of a uniform particle distribution and lack of particle interactions.

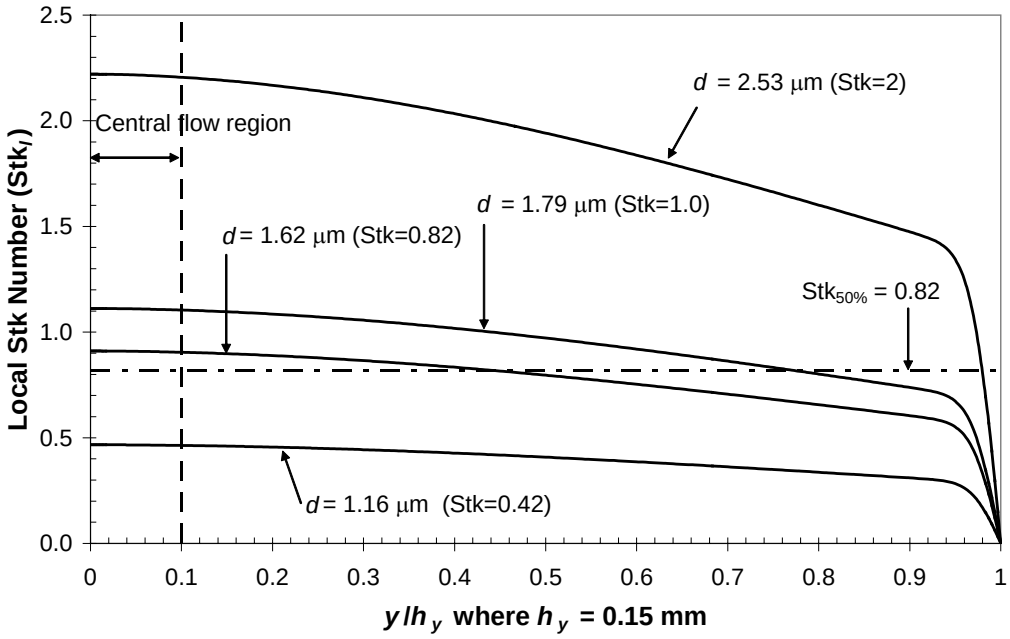

FIGURE 4.3. Local Stokes numbers for smaller particles, based on a converging channel velocity profile for $\dot{Q}_{air}$ = 7.51 × 10^{-5} m^3/s

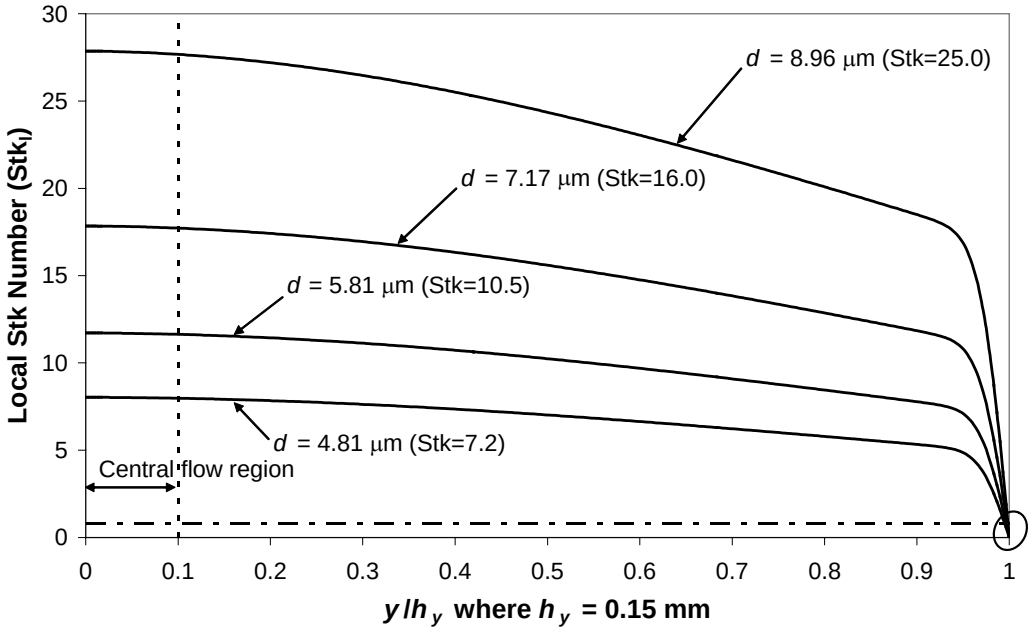

FIGURE 4.4. Local Stokes numbers for larger particles, based on a converging channel velocity profile for $\dot{Q}_{air}$ = 7.51 × 10^{-5} m^3/s

Figure 4.4 show similar results for relatively larger particles ranging from 4.81- to 8.96-μm diameters, and from Stk = 7.2 to 25.0. For larger particles, even though the bulk Stokes number is well above 0.82, a small portion of these particles near the solid wall (y/h_y ~ 1) have very low inertia and consequently a lower local Stokes number. It allows them to enter into the major flows resulting in defect particles. Table 4.1 presents a comparison between measured and calculated collection efficiency, and is seen that there is a fairly acceptable agreement. Certain discrepancies are inherent in predictions using the local Stokes number approach due to potential depletion of particles due to wall effects (discussed later) from the region very close to the solid wall and the effect of non uniform particle distribution. Nevertheless the comparison shows fairly impressive agreement. It is shown that the local Stokes number approach provides reasonable

estimates for the collection efficiency and aids in a better understanding of the physics behind defect occurrences.

TABLE 4.1. Comparison between measured and predicted collection efficiency

d_p [μm]	4.81	7.17	8.96
Measured collecting efficiency (Fig. 3.1)	2.07%	0.06%	0.05%
Predicted collecting efficiency based on the local Stokes number	0.5%	0.21%	0.15%

Characteristics of Convective Transport

From the visualization of the particle transport at various Stokes numbers, transport behavior can be divided in to two categories. These are behavior of particles lesser than the cutoff Stokes number (smaller particle behavior) and those of the larger ones. For smaller Stokes number it is reasonable to assume that the particles follow the flow streamlines very well as shown schematically in figure 4.5a. Here the viscous effects are dominant over the inertial effects. Here, the blank circles represent particle laden in the boundary layer. The gray and the black circles represent those particles laden in the central and outer flow regions respectively. At higher Stokes number, we see that the inertial effects are dominant, causing the particles to break away from the flow streamlines, resulting in crossing trajectories figure 4.5b. This is inline with the visualization results observed in the previous section. We expect all particles, whether laden in the central and outer flow regions, to enter in to the minor flow. Whereas, particles laden in the boundary layer will receive sufficient side impulse to turn in to the major flow due to their low local Stokes number.

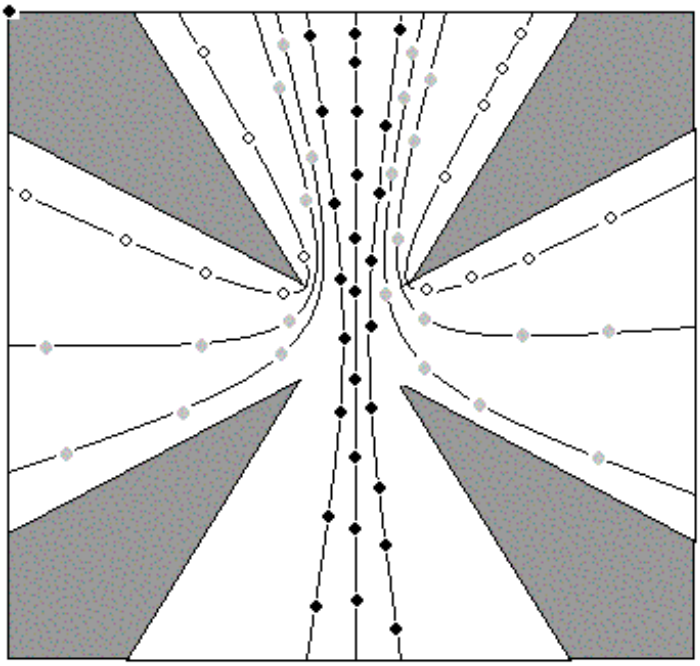

a) Smaller particle behavior (Stk<0.82)

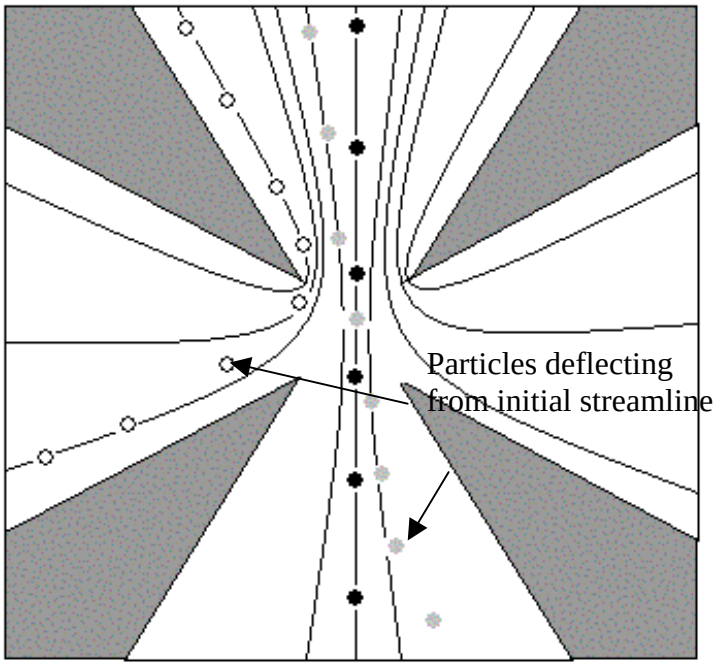

b) Larger particle behavior (Stk>0.82)

FIGURE 4.5. Schematic of particle behavior based on their size (Stokes number)

Mechanism of Clogging in Slit Virtual Impactor – Rectangular Filter Fiber Analogy

We have seen that for mass loadings greater than 1200μg/l rapid clogging of the slit occurs thereby making the device inoperable. Even for lower loading conditions, there is a layer of dust that gets deposited on the slit edge. If the slit edge can be approximated as a single fiber of rectangular cross section as shown in figure 4.6a, we can determine the single fiber collection efficiency. In general, particulate capture in fabric filters occurs by inertial impaction, interception and Brownian diffusion. When Brownian diffusion is insignificant compared with the other two mechanisms, the particle trajectories obtained from deterministic equations of motions can be used for studying the collection efficiency of a rectangular fiber (Zhu et. al., 2000). If we use a control volume as shown in figure 4.6b for the Kuwabara flow field, we can define fiber volume fraction α_f as

$$\alpha_f = \frac{ab}{(b+\frac{w}{2})(a+\frac{w_1}{2})} \tag{4.1}$$

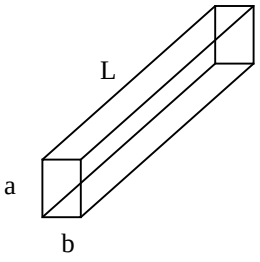

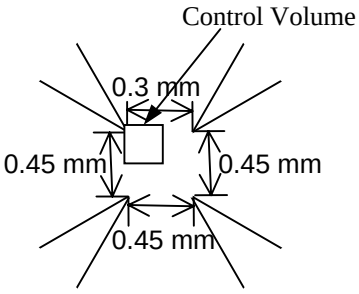

a) Rectangular fiber representation of the slit b) Region under analysis

FIGURE 4.6 Single fiber representation of slit edge and the control volume under investigation

In inertial impaction a particle will be captured when its trajectory ends on fiber surface and in the case of interception, particle capture occurs when trajectories come within one particle radius from the fiber surface. Zhu et al., (2000) suggested using hydraulic diameter for analytical modeling of collection efficiency of a single fiber of rectangular cross section. Hydraulic diameter d_h is defined as the ratio of the four times the cross sectional area to the wetted perimeter. We have

$$d_h = \frac{4ab}{a+2b}, \tag{4.2}$$

where a and b are as shown in figure 4.6. Hinds (1999) gives the expression for collection efficiency due to interception and impaction as

$$\eta_{imp+int} = \frac{(1-\alpha_f)R^2}{Ku(1+R)} + \frac{(Stk)J}{2Ku^2} \tag{4.3}$$

Where, R = d_p/d_h ; $J = (29.6 - 28\alpha_f^{0.62})R^2 - 27.5R^{2.8}$, for R<0.4 and J = 2 for R>0.4.

Ku = Kuwabara number, $Ku = \alpha_f - \frac{\alpha_f^{\ 2}}{4} - \frac{3}{4} - \frac{\ln(\alpha_f)}{2}$ (4.4)

Stk. = Stokes number, $Stk = \frac{\rho_p d_p^2 U}{18\mu d_h}$ (4.5)

When the aspect ratio (a/b) is close to unity, we can approximate the rectangular fiber to a circular one having equivalent hydraulic diameter d_h. The single fiber collection efficiency for a given particle size is give by equation (4.3).

For a polydisperse distribution, the average collection efficiency can be defined as

$$\eta_{i,ave} = \int_0^\infty \tilde{n}(x)\eta_{imp+int,x}dx \tag{4.6}$$

Where $\eta_{imp+int,x}$ is the collection efficiency due to impaction and interception for a particle of size *x*. $\tilde{n}(x)$ is the normalized number distribution function. Most often particle size distributions are normal, log normal or other such distributions. Let us use a log-normal distribution as ARD and most of the precursor powder distributions are of this type as shown in figure 4.7. Normalized log-normal number distribution can be written as

$$\tilde{n}(x) = \frac{1}{x\sqrt{2\pi}\ln\sigma_g}\exp\left(-\frac{(\ln x - \ln CMD)^2}{2(\ln\sigma_g)^2}\right) \tag{4.7}$$

Where CMD ($d_{50\%}$) is the count median diameter and σ_g is the geometric standard deviation. Neglecting the effect of impaction, as 99% of the particles are less than 2.9 micron, the overall collection efficiency for a single fiber due to interception is

$$\eta_{i,ave} = \int_0^\infty \tilde{n}(x)\left(\frac{(1-\alpha_f)R^2}{Ku(1+R)}\right)dx \tag{4.8}$$

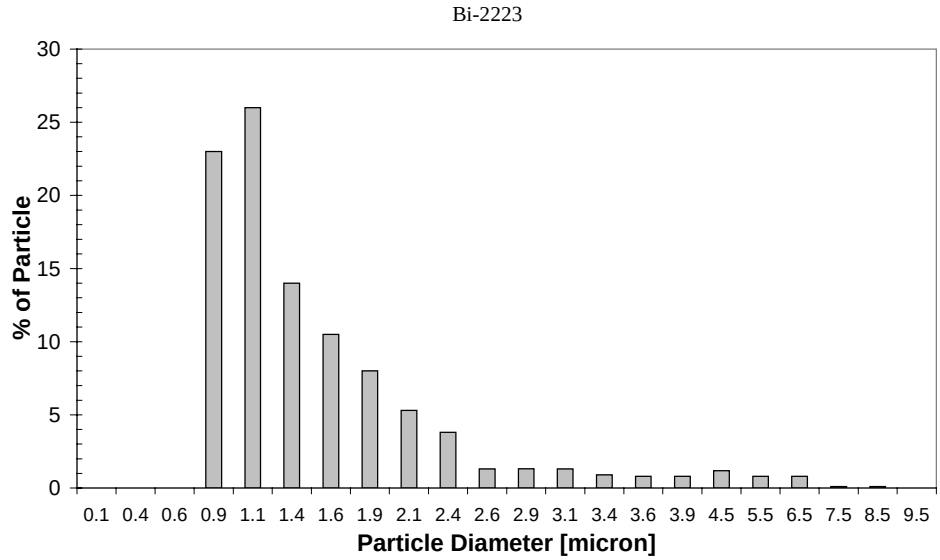

a) Number distribution of Bi-2223 (Source American Superconductor)

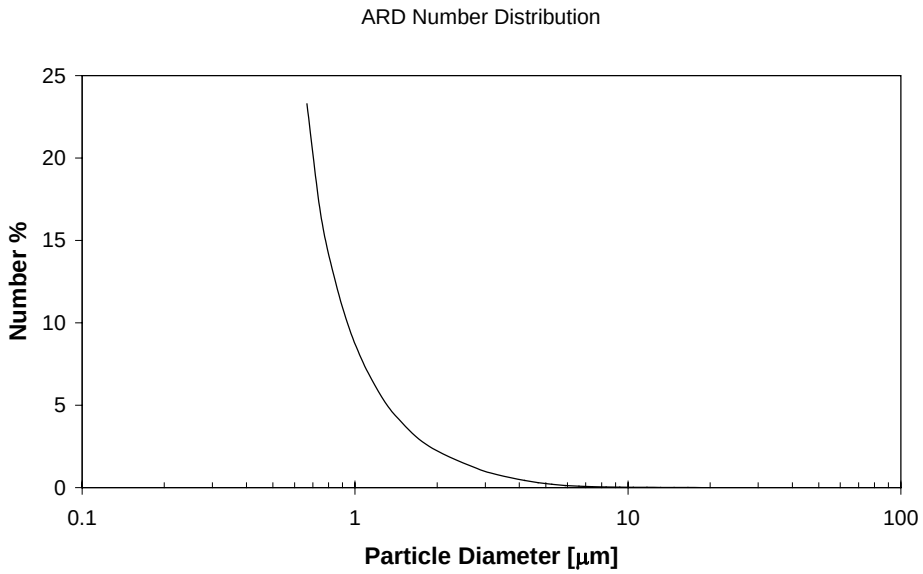

b) Number distribution of ARD (Source Powder Technology Inc.)

FIGURE 4.7. Number distribution plots for ARD and Bi-2223 precursor powder

If the mass loading is 'm' μg/l, then the total mass moving past the slit edge per second would be $\dot{Q}$ x m μg/s, Where $\dot{Q}$ is the volume flow rate. If the device is operated for 't' seconds, the total mass that moved past the slit would be $\dot{Q}$ x m x t μg. Of this mass, the slit wall would intercept $2\eta_{i,ave}$ percent. Total projected surface area occupied by these clogged particles is

$$S = \frac{\left(\dot{Q} \times m \times t \times 6\right) \times (2\eta_{i,ave})}{4\rho_p d_{ave}}, \tag{4.9}$$

where d_{ave} is average particle diameter (Hinds, p87).

For our case,

1.) Let us assume a = b = w/10. Then d_h = 2w/15. = 40 μm (w = 300 μm)

2.) For ARD, d_{ave} = 1.135742μm, CMD = 0.917μm & $d_{84\%}$ = 1.599 μm, ln(σ_g) = 0.5564.

3.) U = 10.6 m/s (Bulk velocity), ρ_p = 2650 Kg/m^3.

4.) Volume fraction α_f = 0.0196

5.) Ku = 1.2354

6.) Particle size range: 0.666 to 89.13 μm

7.) Overall collection efficiency due to interception is 0.148348% (0.074174% per edge)

8.) The design volume flow rate $\dot{Q}$ = 7.52 x 10^{-2} l/s.

The cross-sectional area of slit is 7.62 x 10^{-6} m^2 (0.3mm*2.54cm). We can hypothesize that clogging would occur, if total projected surface area occupied by

particles collected on slit edge is equal to cross-sectional area of the opening. From equation (4.9), we can calculate total time in seconds it would take to clog the slit. Table 4.2 provides a comparison between the calculated and experimentally determined time for clogging. For ARD, we have $t = \frac{137.048 \times 10^3}{m}$.

TABLE 4.2. Clogging time, comparison between experimental and analytical results

S.No	Estimated Mass Loading (μg/l)	Time for clogging (s)	
		Calculated	Experimental
1.)	600	228.41	>300
2.)	1000	137.048	>200
3.)	1300	105.42	120

The following assumptions have been made in the preceding analysis.

1.) Uniform particle distribution across the cross section

2.) Primary mechanism involved is only interception

3.) Fiber aspect ratio is close to one so that a circular fiber approximation is reasonable.

4.) Once a particle gets collected it is not resuspended.

5.) Log normal particle distribution.

CONCLUSION

The transport behavior of solid particles in slit virtual impactor has been studied experimentally and the measured data have been verified using local Stokes number approach. Flow visualization results have shown that particles essentially follow the flow streamlines at lower Stokes numbers. At higher Stokes numbers, inertial effects become dominant, causing the particles to deviate from their initial streamlines. Even though the bulk Stokes number was greater than the cutoff value for larger particles at a given flow rate, the Stokes number at near wall regions was significantly lower due to the slow local velocities. This resulted in particles that are laden in the near wall to get conveyed to the major flow, thereby resulting in a defect occurrence. Monodisperse particles ranging from 1.2 to 9 μm were used to determine collection efficiencies whose transport in the VI were analyzed using digitized images. The measured collection efficiencies, as shown in figure 3.1, shows a fairly close agreement with the values estimated using the local Stokes number approach.

Generation of particles of monodisperse size was critical to the success of this experimental investigation. A Vibrating Orifice Aerosol Generator designed and built in the lab generated particles of uniform size with an average standard deviation of less than 0.5 micron, which enabled accurate characterization of impactor cutoff. Dry dispersion turntable aerosol generator, also designed and built in the lab, provided with a uniform dust output for mass loading experiments. It had good variability and control. Various mass loadings could be obtained by either varying turntable speed or inlet pressure or both.

This study is the first to address the performance of a slit virtual impactor from a single particle basis. Real time monitoring of particle transmission gives a good understanding of the physics of particle transport that were so far confined to theoretical and numerical analyses. This research has successfully identified the sources of individual defect occurrences and provision for sheath airflow was suggested to achieve a defect free separation. For a viable commercial operation, VI's performance at higher mass loadings was evaluated. Clogging of the silt due to particle wall interaction effects hindered operation of the VI at higher mass loadings. A method to analytically estimate the time to clog, given an initial loading condition and particle size distribution, has been developed by approximating the slit edge to a rectangular filter fiber. Even for lower mass loadings, it was seen that clogging would occur as long as there were wall interceptions. Thus it would be necessary to provide sheath airflow to prevent clogging and defect particle transmission.

Particle size is critical to a number of applications including powder in tube processing for superconducting wire fabrication. Other applications where larger particles would ruin the products are in production of dielectric ceramics, UV-sun block face creams etc. Current powder processing techniques for these applications are rather expensive both money wise and time wise. This research was carried out with a view to develop a commercially viable and effective powder processing technique. With suggested modifications, this technique would be a viable alternative to current powder processing techniques like sieving.

REFERENCES

Chao, Z., Chao, H.L., Chun, S.C.(2000): Inertial Impaction-Dominated Fibrous Filtration with Rectangular or Cylindrical Fibers. *Powder Technology.* 112:149-162

Chen, B.T. and Yeh, H.C. (1987). An Improved Virtual Impactor: Design and Performance. *J. Aerosol Sci.* 18:203-214

Ding, Y., Koutrakis, P. (2000). Development of a Dichotomous Slit Nozzle Virtual Impactor. *J. Aerosol Sci.* 31:1421-1431

Fu, X., Gupta, A., McIntyre, P.M., Phares, D.J. (2003). New Size Sorting Technology for Superconducting Powders. *IEEE Transactions on Applied Superconductivity* 13: 3494-3497

Fuchs, N.A. (1964). *The Mechanics of Aerosols*. Pergamon Press, New York, p.154

Gotoh, K. and Masuda, H. (2000). Improvement of the Classification Performance of a Rectangular Jet Virtual Impactor. *Aerosol Sci. Tech.* 32:221-232

Guo, Y.C., Li, J.N., Yavuz, M., Liu, H.K. and Dou, S.X. (1995) Effect of Precurssor Powder on the Properties of Superconducting Wires and Tapes. *Advances in Cryogenic Engineering.* 42:751-755

Hecht, E. (1998). *Optics*. Addison-Wesley Pub. Co., Reading, MA, p.105

Han, R. and Moss, O.R. (1997). Flow Visualization Inside a Water Model Virtual Impactor. *J. Aerosol Sci.* 28:1005-1014

Hinds W.C.(1999) *Aerosol Technology.* John Wiley & Sons, New York, p.75-93

Lee, P., Chen, D.R. and Pui, Y.H. (2003). Experimental Study of a Nanoparticle Virtual Impactor. *J. Nanoparticle Research.* 5:260-280

Levendis, Y.A. and Flagan R.C. (1989). Synthesis, Formation and Characterization of Micron Sized Glassy Carbon Spheres of Controlled Pore Structure. *Carbon.* 27:265-283

Loo, B.W. and Adachi, R.S. (1979). A Second Generation Dichotomous Sampler for Large Scale Monitoring of Airborne Particulate Matter. *Lawrence Berkeley Lab Report*. LBL-8725.

Loo, B.W. and Cork, C.P. (1988). Development of High Efficiency Virtual Impactors. *Aerosol Sci. Tech.* 9:167-176

Marple, V.A. and Chein, C.M. (1980). Virtual Impactors: A Theoretical Study. *Environ. Sci. Tech.* 14:975-986

Oberdorster, G. and Utell, M.J. (2002). Ultrafine Particles in the Urban Air: To the Respiratory Tract - And Beyond? *Environ Health Persp.* 110: A440-A441

Pope, C.A., Bates, D.V. and Raizenne, M.E. (1995). Health Effects of Particulate Air Pollution, Time for Reassessment. *Environ Health Persp.* 103:472-480

Sioutas, C., Koutrakis, P. and Burton, R.M. (1994). Development of a Low Cutpoint Slit Virtual Impactor for Sampling Ambient Fine Particles. *J. Aerosol Sci.* 25:1321-1330

VITA

Satyanarayanan Seshadri was born on the 8th of May 1981 in Madras, India. He obtained a Bachelor of Engineering degree with distinction in mechanical engineering from the University of Madras, Madras, India in 2002. He came to Texas A&M University, Department of Mechanical Engineering in the fall of 2002 and started working with the research group of Dr. Phares in the spring of 2003. His research interests include fundamental particle motion in inertial separation devices, air pollution studies, using optical diagnostic techniques for performance evaluation of particle classification devices etc. His favorite pastime is peeking in the future with the zodiac as the map and Vedic astrological techniques as the telescope.

He can be reached permanently at 107, Canal bank rd., Indira Nagar, Adyar, Madras, India 60020. He can be e-mailed at satya1981@hotmail.com.